Available online at www.sciencedirect.com

SciVerse ScienceDirect

Advances in Space Research 51 (2013) 1047–1064

ADVANCES IN SPACE RESEARCH (a COSPAR publication)

www.elsevier.com/locate/asr

Review

Geocenter coordinates estimated from GNSS data as viewed by perturbation theory

Michael Meindl *, Gerhard Beutler, Daniela Thaller, Rolf Dach, Adrian Jäggi

Astronomical Institute, University of Bern, Sidlerstrasse 5, 3012 Bern, Switzerland

Received 26 May 2012; received in revised form 29 October 2012; accepted 31 October 2012
Available online 9 November 2012

Abstract

Time series of geocenter coordinates were determined with data of two global navigation satellite systems (GNSSs), namely the U.S. GPS (Global Positioning System) and the Russian GLONASS (Global'naya Nawigatsionnaya Sputnikowaya Sistema). The data was recorded in the years 2008–2011 by a global network of 92 permanently observing GPS/GLONASS receivers. Two types of daily solutions were generated independently for each GNSS, one including the estimation of geocenter coordinates and one without these parameters.

A fair agreement for GPS and GLONASS was found in the geocenter x- and y-coordinate series. Our tests, however, clearly reveal artifacts in the z-component determined with the GLONASS data. Large periodic excursions in the GLONASS geocenter z-coordinates of about 40 cm peak-to-peak are related to the maximum elevation angles of the Sun above/below the orbital planes of the satellite system and thus have a period of about 4 months (third of a year). A detailed analysis revealed that the artifacts are almost uniquely governed by the differences of the estimates of direct solar radiation pressure (SRP) in the two solution series (with and without geocenter estimation). A simple formula is derived, describing the relation between the geocenter z-coordinate and the corresponding parameter of the SRP. The effect can be explained by first-order perturbation theory of celestial mechanics. The theory also predicts a heavy impact on the GNSS-derived geocenter if once-per-revolution SRP parameters are estimated in the direction of the satellite's solar panel axis. Specific experiments using GPS observations revealed that this is indeed the case.

Although the main focus of this article is on GNSS, the theory developed is applicable to all satellite observing techniques. We applied the theory to satellite laser ranging (SLR) solutions using LAGEOS. It turns out that the correlation between geocenter and SRP parameters is not a critical issue for the SLR solutions. The reasons are threefold: The direct SRP is about a factor of 30–40 smaller for typical geodetic SLR satellites than for GNSS satellites, allowing it in most cases to not solve for SRP parameters (ruling out the correlation between these parameters and the geocenter coordinates); the orbital arc length of 7 days (which is typically used in SLR analysis) contains more than 50 revolutions of the LAGEOS satellites as compared to about two revolutions of GNSS satellites for the daily arcs used in GNSS analysis; the orbit geometry is not as critical for LAGEOS as for GNSS satellites, because the elevation angle of the Sun w.r.t. the orbital plane is usually significantly changing over 7 days.

Keywords: Geocenter; Solar radiation pressure; Celestial mechanics; Perturbation theory; GNSS; SLR

* Corresponding author. Present address: ETH Zurich, Institute of Geodesy and Photogrammetry, Schafmattstrasse 34, 8093 Zurich, Switzerland.
E-mail address: mmeindl@ethz.ch (M. Meindl).

0273-1177/$36.00 © 2012 COSPAR. Published by Elsevier Ltd. All rights reserved.
http://dx.doi.org/10.1016/j.asr.2012.10.026

Contents

1. Introduction

1.1. Basics

The satellite geodetic methods used for highest accuracy applications determine the distances between satellites orbiting the Earth's center of mass and receivers (observatories) on the Earth's surface based on the measurement of propagation times of electromagnetic signals. In rough approximation we may write

$$\mathcal{D} = |\boldsymbol{r}(t) - (\boldsymbol{R}(T) - \boldsymbol{G}(T))| + \mathcal{E}, \tag{1}$$

where $\mathcal{D}$ stands for the distance derived from the measurements, $\boldsymbol{r}$ for the geocentric position vector of the satellite, $\boldsymbol{R}$ for the position vector of the observer w.r.t. the origin of the reference system, and $\boldsymbol{R}$–$\boldsymbol{G}$ for the observer's geocentric position vector; $\boldsymbol{G}$ consequently is the position vector of the geocenter w.r.t. the origin of the reference system (the satellites are forced to revolve around the endpoint of $\boldsymbol{G}$). The epochs t and T depend on the measurement technique: For global navigation satellite systems (GNSS) they are signal emission and reception times, respectively, for satellite laser ranging (SLR) $t = T$ is the time of reflection of the laser pulse at the satellite.

Depending on the observation technique, the term $\mathcal{E}$ may contain signal delays caused by the Earth's neutral and electrically charged atmosphere; satellite and receiver clock corrections w.r.t. a reference clock (e.g., a particular GNSS system time); sensor offsets (e.g., optical centers of SLR reflectors or microwave antenna phase centers) w.r.t. the center of mass of a satellite or w.r.t. a terrestrial geodetic marker; technique-specific biases, e.g., SLR range biases or GNSS phase ambiguity parameters.

Eq. (1) is fundamental to determining the coordinates of the geocenter (and other parameters) for all observation techniques. The equation contains scalar products of vectors and is therefore not attached to a particular coordinate system. The vectors in Eq. (1) may, however, also be interpreted as component matrices of the coordinates of vectors $\boldsymbol{r}$, $\boldsymbol{R}$, and $\boldsymbol{G}$, referring to a particular coordinate system.

An Earth-fixed reference frame is advantageously chosen for the estimation of the geocenter coordinates, because the coordinates of the vectors $\boldsymbol{R}(T) = \boldsymbol{R}$ and $\boldsymbol{G}(T) = \boldsymbol{G}$ are time-independent in this case (assuming a rigid Earth). Consequently, the vector $\boldsymbol{r}(t)$ has to be available in (or transformed into) the terrestrial reference frame. In our analysis, the coordinates of the reference stations refer to the ITRF2008 (International Terrestrial Reference Frame, Altamimi et al., 2011).

Introducing $\boldsymbol{\mathcal{T}} \stackrel{\text{def}}{=} \boldsymbol{r} - (\boldsymbol{R} - \boldsymbol{G})$ as the topocentric satellite position vector, the partial derivatives of the distance $\mathcal{D}$ in Eq. (1) w.r.t. the geocenter coordinates in the Earth-fixed reference frame may be written as

$$\frac{\partial \mathcal{D}}{\partial G_i} = \sum_{k=1}^{3} \frac{\partial \mathcal{D}}{\partial \mathcal{T}_k} \frac{\partial \mathcal{T}_k}{\partial G_i} = \frac{\mathcal{T}_i}{|\boldsymbol{\mathcal{T}}|} \quad \text{with} \quad i = 1, 2, 3. \tag{2}$$

The $\mathcal{T}_{i/k}$ are the components of vector $\boldsymbol{\mathcal{T}}$ in the used coordinate system and G_i the components of vector $\boldsymbol{G}$. The partial derivative of the observation $\mathcal{D}$ w.r.t. the

coordinate G_i of the geocenter thus simply is the component i of the unit vector associated with the topocentric vector $\mathcal{T}$.

Eq. (2) is the partial derivative entering the normal equation system (NEQ) when analyzing SLR observations. The analysis of GNSS observations is complicated by epoch-specific satellite and receiver clock errors, which have to be pre-eliminated at each epoch. Instead of pre-eliminating these errors one may analyze the difference between simultaneous observations either made (a) by two different sites to the same satellite (which greatly reduces the satellite clock errors) or (b) by the same site to two different satellites (which eliminates the receiver clock errors). The partial derivative of a type-(a) difference w.r.t. the geocenter coordinates simply is the difference of two partial derivatives of type (2):

$$\frac{\partial(\mathcal{D}_1 - \mathcal{D}_2)}{\partial G_i} = \frac{\mathcal{T}_{1,i}}{|\boldsymbol{\mathcal{T}}_1|} - \frac{\mathcal{T}_{2,i}}{|\boldsymbol{\mathcal{T}}_2|} \quad \text{with} \quad i = 1, 2, 3, \tag{3}$$

where the $\mathcal{D}_{1/2}$ are the observations pertaining to the two sites and the $\boldsymbol{\mathcal{T}}_{1/2}$ the corresponding topocentric position vectors. The absolute values of the partial derivatives (2) are much larger than these of the partial derivatives (3), because the topocentric distances of satellites usually are much larger than the distances between receivers. The sensitivity of the GNSS observable w.r.t. the geocenter coordinates is thus greatly reduced when compared to SLR. Note that the comparison of Eqs. (2) and (3) may really only serve as an order of magnitude argument. A mathematically correct treatment of the GNSS case requires to process all simultaneous observations of the tracking network in the same analysis step and to take the mathematical correlations between them into account. Note, as well, that differences of type (b) do not substantially reduce the sensitivity w.r.t. the geocenter coordinates.

1.2. Geocenter determination using different observation methods

When speaking of the geocenter we mean the difference between the center of mass of the entire system Earth (including solid Earth, atmosphere, oceans, hydrosphere, cryosphere) and the origin of a terrestrial reference frame, e.g., the ITRF at a given epoch. As satellite orbits refer to the center of mass, the geocenter can be determined by satellite observation techniques.

Variations of the geocenter are caused by mass redistributions in the system Earth. Annual and semi-annual periods are predominant (Dong et al., 1997). These variations can be explained by geophysical models for the atmosphere, oceans and hydrology. In 1997, the International Earth Rotation and Reference Systems Service conducted an analysis campaign dedicated to the determination of the geocenter. The status at that time is summarized by Ray (1999). Meanwhile, the geocenter series derived from geophysical models and from space-geodetic data have been compared in several articles, e.g., by Chen et al. (1999), Bouillé et al. (2000), Moore and Wang (2003), Feissel-Vernier et al. (2006), and Wu et al. (2012). All studies show a good agreement between geophysical models and space geodetic results, with annual amplitudes of about 2–3 mm for the x- and y-components and about 3–5 mm for the z-component.

The best geocenter time series are based on the SLR solutions. SLR measurements to the geodetic satellites LAGEOS-1 and -2 are particularly well suited for geocenter estimation:

- The absolute and unambiguous observations provide sub-centimeter accuracy for so-called normal points since decades;
- the propagation delays of the SLR pulses caused by the Earth's atmosphere may be taken into account with sub-centimeter accuracy by well-established models (Mendes and Pavlis, 2004) without solving for atmosphere-related parameters;
- non-gravitational forces acting on the satellites are easily modeled because atmospheric drag may be neglected at the height of the LAGEOS satellites and solar radiation pressure (SRP) may be accounted for on the sub-centimeter level without solving for model parameters;
- parameter estimation may be based on relatively long arcs—seven-day arcs corresponding to more than 50 revolutions are standard—helping to de-correlate parameters of different kinds.

The Earth's geocenter, as established by SLR observations of the LAGEOS satellites, is rather stable over long time spans (years to decades). Variations in the SLR-derived time series are within 1 cm for the x- and y-components and within about 1.5 cm for the z-component.

Watkins and Eanes (1997) demonstrate that even diurnal and sub-diurnal variations induced by tides might be determined by LAGEOS solutions although their size is at the few millimeter level.

Alternatively, the other two satellite techniques, i.e., GNSS and the French Doppler Orbitography and Radiopositioning Integrated by Satellite (DORIS) may be used for geocenter determination. The two methods are attractive, because much denser global observing networks (and thus many more observations) are available than for SLR. In the case of GNSS this is counterbalanced (a) by a reduced sensitivity of the basic observable w.r.t. the geocenter coordinates (see Section 1.1); (b) by the presence of phase ambiguity parameters (which may, however, be resolved to integer numbers to a large extent in a refined analysis); and (c) by the necessity to estimate troposphere-related parameters. Last but not least, GNSS and DORIS satellites are far from having a spherical shape, implying that SRP parameters have to be determined in the analysis. Needless to say that light–shadow transitions are more complicated to model, as well, for non-spherical satellites.

Despite these obstacles there recently were quite a few determinations of the geocenter based on microwave

observation techniques—without having been able so far to replace the SLR-derived geocenter time series as the gold standard. The determination of the z-coordinate of the geocenter, i.e., of the coordinate G_3 of vector $\boldsymbol{G}$, proved to be particularly delicate. Using the SLR solutions as reference, it is relatively easy to single out artifacts in geocenter time series established by other observation techniques. Let us briefly mention some of the recent articles related to geocenter determinations.

Ferland and Piraszewski (2009) describe the procedure of the International GNSS Service (IGS, Beutler et al., 1999; Dow et al., 2009) to regularly produce a realization of the ITRF. This activity includes the estimation of the geocenter, called in that article *apparent* geocenter, for all contributing analysis centers and for the combined solution. The attribute *apparent* is used to reflect the limitations caused by SRP modeling. The reconstruction of the geocenter is possible, because the products of the IGS analysis centers are provided in a particular format allowing it to remove possible constraints on the individual network solutions, to redefine the geodetic datum, and to solve in particular for a common offset of the ITRF reference sites. The geocenter estimates are (implicitly) compared to the SLR realization of the geocenter. The consistency of the individual solutions w.r.t. the mean and of the mean w.r.t. the SLR-defined geocenter are of the order of 5 mm for the x- and y-components and of the order of 10 mm for the z-component. These accuracies and consistencies are remarkable achievements of the IGS.

Lavallée et al. (2006) introduce a novel approach to derive geocenter coordinates by taking into account two methods in a combined way: the classical network translation approach on one hand and the degree-one coefficients derived from surface load deformations of the observing stations on the other hand. The authors show that both approaches have deficiencies, especially for GPS solutions, when applied independently. The unified approach, considering both types of geocenter estimation, proved to reduce the discrepancies between individual GPS solutions and to increase the agreement of the annual signals in the GPS solutions with those of the SLR-derived series.

Gobinddass et al. (2009) provide a profound analysis related to DORIS: Measurement noise and systematic errors in the time series of G_3 prove to be about ten times larger than the level achieved by SLR. The problems can be clearly attributed to the SRP models, in particular to the estimation of radiation pressure parameters.

Kang et al. (2009) use the observations of the on-board GPS receivers of the GRACE-A and -B satellites and a global tracking network of GPS receivers to determine the Earth's geocenter. The geocenter coordinates are estimated together with the GRACE satellites' initial position and velocity vectors, once-per-revolution (OPR) empirical acceleration parameters (set up in along- and cross-track directions), and GPS-specific parameters like phase ambiguities and tropospheric zenith path delays. The results are remarkable. Amplitudes and phases of the results are low-pass filtered to monthly moving averages. Fitting these filtered values by an annual signal results in geocenter time series of rather good quality in all three coordinates—even when compared to the SLR series.

Wu et al. (2012) review geocenter motion and its geodetic and geophysical implications in a very broad sense. The geodesy-related prospects in the discussion section summarize the state-of-the-art of satellite-geodetic geocenter determination and of its current limitations. Once more, the SRP model is suspected to be the accuracy-limiting factor for microwave techniques.

Thaller et al. (in press) study the combination of microwave and SLR observations of GNSS satellites and of the classical geodetic satellites LAGEOS and ETALON. It becomes apparent that the SLR observations to the GNSS satellites could not substantially improve the GNSS solutions, whereas the combination of the SLR NEQs resulting from the LAGEOS and ETALON observations with the GNSS NEQs gave substantial improvements—in particular when the SRP model for the GNSS satellites was modified (and weakened). The authors conclude—in agreement with the other references cited here—that the SRP model plays an essential role for the biases in GNSS-derived geocenter series. We will come back to a particular aspect of this article in Section 5.1.

Our work differs from the cited articles by putting the emphasis on the problems of estimating the geocenter coordinates, in particular of G_3, using GPS and/or GLONASS (and not on geophysical aspects). We explain the problems caused by the correlation between particular parameters of the orbit model and the geocenter coordinate G_3 using first-order perturbation theory. Before revealing the motivation for our investigations in Section 1.4 we briefly introduce the solution series used in our analysis in Section 1.3.

1.3. GNSS solution series generated for this article

The series of geocenter coordinates analyzed in this article are based on Meindl (2011), which contains a detailed description of the data used, the analysis scheme applied, and the solutions generated.

A global network of 92 combined GPS/GLONASS receivers was selected, which in essence permanently collected the observations of all active GPS and GLONASS satellites in the years 2008–2011 (the data from 2011 was added for this study). Special care was taken to keep the GPS and GLONASS solutions comparable, to the extent possible. Unfortunately, the GLONASS was still far from being complete in 2008, which is why only the years 2009–2011 resulted in high-quality solutions for GLONASS. Nevertheless, the year 2008 was kept in the analysis to rule out data quality as an explanation for some excursions in the geocenter time series.

All calculations were performed with the latest development version of the Bernese GPS Software (Dach et al., 2007). Up-to-date models were applied and the data analysis closely followed the processing scheme used by the

Center for Orbit Determination in Europe (CODE) for its contribution to the IGS final product line.

1.4. Motivation

Fig. 1, showing the time series of the geocenter coordinate G_3, as estimated by GPS (top) and GLONASS (bottom), motivated the present study. It is contained in this form in Meindl (2011). From the fact that there is no similarity between Fig. 1 (top) and (bottom) we must conclude that there are artifacts at least in one of the solutions. In view of the fact that the GLONASS-derived coordinates G_3 are much larger than those emerging from GPS and that there is an eye-catching correlation between the big excursions and the maximum and minimum values of β_s, the Sun's elevation above/below the orbital planes, we conclude that the GLONASS estimates are dominated by artifacts.

Fig. 1 (bottom) was the motivation to study the relationship between the orbit parameters and the geocenter in greater detail because the correlation between G_3 and the angle β_s clearly suggests a correlation with one of the estimated orbit parameters or with a linear combination thereof.

Fig. 2 shows that the x- and y-coordinates of the geocenter are consistent for GPS and GLONASS. The poor GLONASS data quality in the year 2008 explains some discrepancies between the GPS- and GLONASS-derived series. The noise is obviously significantly larger for the GLONASS than for the GPS solution—this aspect is in particular important in the year 2008. With the naked eye one would claim to see an annual (or quasi-annual) signal but there are no obvious correlations with the angles β_s. For the time being, we therefore decided not to study the correlations between the x- and y-coordinates of the geocenter on one hand and the orbital parameters on the other hand.

Fig. 2 (bottom) once again shows the unrealistically large variations of the GLONASS-derived coordinates G_3 compared to the GPS-derived values. Fig. 2 also contains the results of a combined GPS/GLONASS solution, which was established on the observation level (Meindl, 2011). The combination follows more or less the GPS-only solution, indicating that GPS is much stronger for the purpose

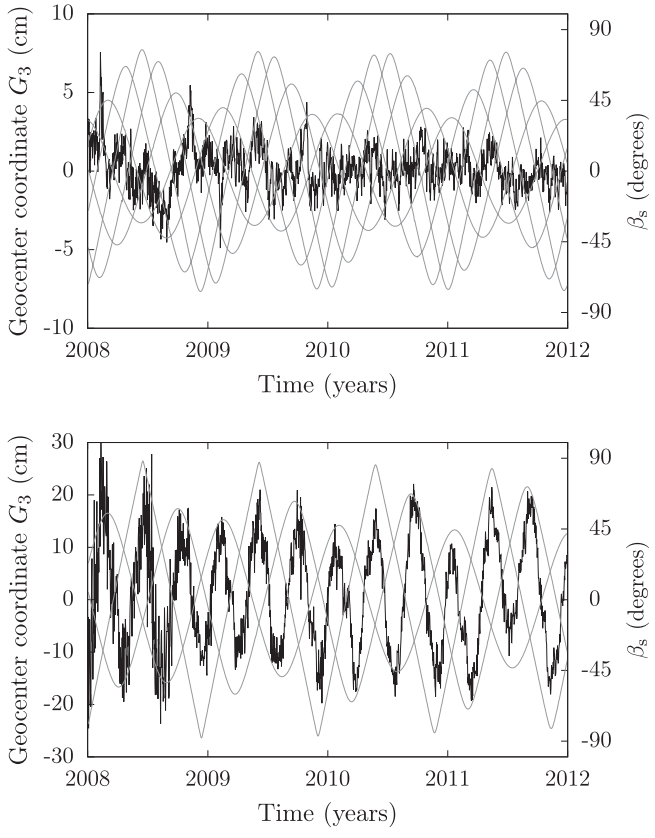

Fig. 1. Coordinate G_3 estimated by GPS (top) and GLONASS (bottom) and elevation β_s of the Sun above/below the orbital planes.

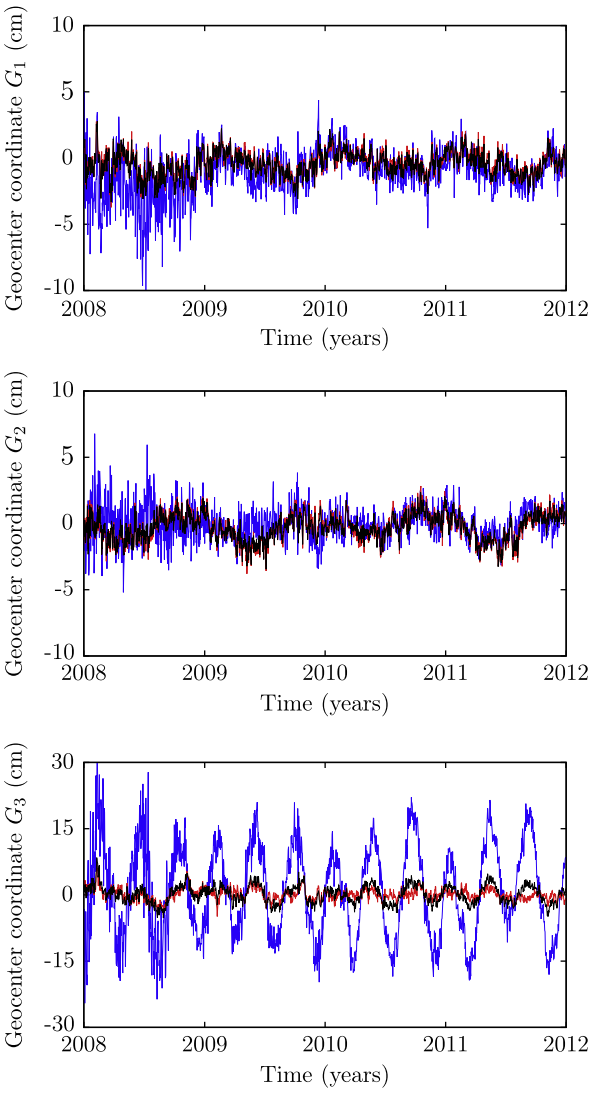

Fig. 2. Geocenter coordinates estimated by GPS (red), GLONASS (blue), and by a GPS/GLONASS combination (black): G_1 (top), G_2 (center), G_3 (bottom).

of geocenter estimation. Note, however, that the coordinates G_3 from the combined solution (Fig. 2, bottom) still show traces of the GLONASS excursions. It is problematic that an artifact of the GLONASS solution is present in the combined solution—and as a matter of fact dominates the signature of (the second half of) the time series.

2. Orbit parametrization and empirical solar radiation pressure model

2.1. Orbit model

The six osculating orbital elements a, e, i, Ω, ω, and T_0 at the initial epoch t_0 characterize a particular satellite orbit. Fig. 3 illustrates the elements (showing the argument of latitude u instead of T_0). The semi-major axis a and the numerical eccentricity e define the size and shape of the orbit; the orientation of the orbit is determined by the inclination i w.r.t. the equatorial plane, the right ascension of the ascending node Ω, and the argument of perigee ω; the perigee passing time T_0, or the initial argument of latitude $u(t_0)$, is required to define the satellite's position within the orbit at arbitrary times.

The empirical part of the orbit model used here and by the CODE analysis center is based on the decomposition of the solar radiation pressure (SRP) accelerations into three orthogonal directions represented by the unit vectors

$$\boldsymbol{e}_\mathrm{D} \overset{\text{def}}{=} \frac{\boldsymbol{r}_\mathrm{s}-\boldsymbol{r}}{|\boldsymbol{r}_\mathrm{s}-\boldsymbol{r}|}, \quad \boldsymbol{e}_\mathrm{Y} \overset{\text{def}}{=} -\frac{\boldsymbol{e}_r \times \boldsymbol{e}_\mathrm{D}}{|\boldsymbol{e}_r \times \boldsymbol{e}_\mathrm{D}|}, \quad \text{and} \quad \boldsymbol{e}_\mathrm{X} \overset{\text{def}}{=} \boldsymbol{e}_\mathrm{D} \times \boldsymbol{e}_\mathrm{Y}, \tag{4}$$

where $\boldsymbol{r}_\mathrm{s}$ and $\boldsymbol{r}$ are the geocentric vectors of the Sun and the satellite and $\boldsymbol{e}_r$ is the unit vector associated with vector $\boldsymbol{r}$. The unit vectors $\boldsymbol{e}_\mathrm{D}$ and $\boldsymbol{e}_\mathrm{Y}$ point from the satellite to the Sun and along the satellite's solar panel axes, respectively. The total acceleration of a satellite due to SRP is given by

$$\boldsymbol{a}_\mathrm{srp} = \boldsymbol{a}_{\mathrm{srp},0} + D(u)\,\boldsymbol{e}_\mathrm{D} + Y(u)\,\boldsymbol{e}_\mathrm{Y} + X(u)\,\boldsymbol{e}_\mathrm{X}, \tag{5}$$

with

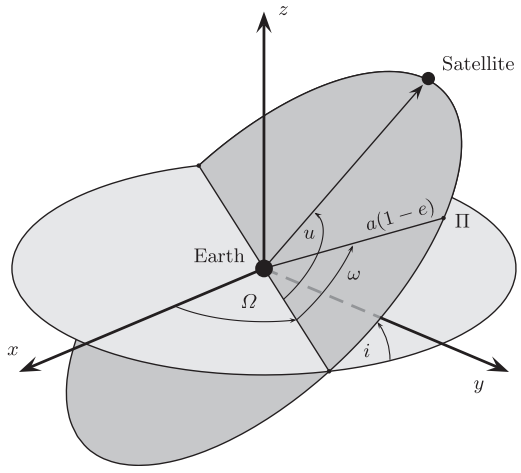

Fig. 3. The orbital elements a, e, i, Ω, ω, and the argument of latitude u (Π marks the perigee of the orbit).

$$\begin{aligned} D(u) &= D_0 + D_\mathrm{c}\cos u + D_\mathrm{s}\sin u, \\ Y(u) &= Y_0 + Y_\mathrm{c}\cos u + Y_\mathrm{s}\sin u, \\ X(u) &= X_0 + X_\mathrm{c}\cos u + X_\mathrm{s}\sin u. \end{aligned} \tag{6}$$

The decomposition (4) and the SRP model (5), (6) were first proposed by Beutler et al. (1994) and are used since that time by the CODE analysis center. The model was refined by Springer et al. (1999) to contain a rather complex a priori model $\boldsymbol{a}_{\mathrm{srp},0}$. The model contains nine parameters: constant accelerations (D_0, Y_0, X_0) and periodic once-per-revolution (OPR) terms $(D_{\mathrm{c/s}}, Y_{\mathrm{c/s}}, X_{\mathrm{c/s}})$ in each of the three directions (4). Additional information is available in Dach et al. (2009).

We follow the standard adopted by CODE and parameterize each orbital arc with six osculating elements at the initial epoch (cf. Fig. 3), with three constant SRP parameters D_0, Y_0, X_0, and with the two OPR parameters $X_{\mathrm{c/s}}$ in the $\boldsymbol{e}_\mathrm{X}$-direction. Consequently, we estimate eleven orbit parameters per satellite per arc. Note that we did not use the a priori model neither for GPS nor for GLONASS (i.e., $\boldsymbol{a}_{\mathrm{srp},0} = \boldsymbol{0}$ for all solutions) as experiments showed that the a priori model has virtually no impact on the estimated geocenter coordinates.

2.2. Decomposition of the solar radiation pressure constituents

The perturbation equations in the Gaussian formulation (see Beutler, 2005, Vol I, Eq. 6.88) assume that the perturbing accelerations are expressed in an orbital system with its first axis $\boldsymbol{e}_\mathrm{R}$ pointing from the geocenter to the satellite. The second axis $\boldsymbol{e}_\mathrm{S}$ is normal to $\boldsymbol{e}_\mathrm{R}$, lies in the orbital plane and points (in particular for the almost circular GNSS orbits) roughly in the direction of satellite motion. The third axis $\boldsymbol{e}_\mathrm{W}$ is normal to the osculating orbital plane. The components of a perturbing acceleration in this rotating coordinate system are designated by R, S, and W. In this section we provide the (R,S,W)-components associated with the constant accelerations of the empirical SRP model (6). The periodic OPR (R,S,W)-components might then be derived easily if required.

The constant perturbing acceleration in $\boldsymbol{e}_\mathrm{D}$-direction is by far the dominating component of the empirical orbit model with $D_0 \approx -0.9 \cdot 10^{-7}\,\mathrm{m/s^2}$ for GPS and $D_0 \approx -1.5 \cdot 10^{-7}\,\mathrm{m/s^2}$ for GLONASS satellites. For reference we note that $D_0 \approx -3.2 \cdot 10^{-9}\,\mathrm{m/s^2}$ for the LAGEOS satellites, i.e., about hundred times smaller than for the GNSS satellites due to the much smaller area-to-mass ratio.

The D-component is dominated by the direct SRP acting on the solar panels, which should always be perpendicular to $\boldsymbol{e}_\mathrm{D}$. This is why the component along $\boldsymbol{e}_\mathrm{D}$ is not varying much over one year. Following Beutler (2005, Vol. II, Eq. 3.151) we may write the direct SRP as

$$\begin{pmatrix} R_\mathrm{D} \\ S_\mathrm{D} \\ W_\mathrm{D} \end{pmatrix} = D \begin{pmatrix} \cos\beta_\mathrm{s}\cos(u-u_\mathrm{s}) \\ -\cos\beta_\mathrm{s}\sin(u-u_\mathrm{s}) \\ \sin\beta_\mathrm{s} \end{pmatrix}, \tag{7}$$

where $-90^\circ \leqslant \beta_s \leqslant 90^\circ$ is the elevation angle of the Sun above/below the orbital plane, u_s is the argument of latitude of the Sun in the satellite's orbital plane, and u is the argument of latitude of the satellite. The geometry of the perturbation is illustrated in Beutler (2005, Vol. II). For $\beta_s = \pm 90^\circ$ one has $R_D = S_D = 0$ and $W_D = \pm D$, i.e., the direct SRP becomes a net out-of-plane acceleration:

$$\begin{pmatrix} R_D \\ S_D \\ W_D \end{pmatrix}_{\pm 90^\circ} = D \begin{pmatrix} 0 \\ 0 \\ \pm 1 \end{pmatrix}. \tag{8}$$

The maximum angles $|\beta_s|$ vary for different GNSS depending on the inclination i of the orbits. The general formula reads:

$$|\beta_s| \leqslant i + \epsilon, \tag{9}$$

where ϵ is the obliquity of the ecliptic. For GPS with $i = 55^\circ$ we therefore have

$$|\beta_s| \leqslant 78.5^\circ \tag{10}$$

and for GLONASS with $i = 64.8^\circ$ we get

$$|\beta_s| \leqslant 88.3^\circ. \tag{11}$$

The direct SRP becomes almost uniquely an out-of-plane acceleration for the maximum angles β_s in the case of GLONASS, whereas significant R_D- and S_D-accelerations remain for GPS.

Using Eqs. (4) and (7) the (R,S,W)-decomposition for the constant Y-acceleration may be easily calculated:

$$\begin{pmatrix} R_Y \\ S_Y \\ W_Y \end{pmatrix} = Y \begin{pmatrix} 0 \\ \frac{\sin\beta_s}{\sqrt{1-\cos^2\beta_s\,\cos^2(u-u_s)}} \\ \frac{\cos\beta_s\,\sin(u-u_s)}{\sqrt{1-\cos^2\beta_s\,\cos^2(u-u_s)}} \end{pmatrix}. \tag{12}$$

The pre-factor Y is commonly called Y-bias. The R-component is zero by construction. The S-component is constant in along-track direction for $\beta_s = \pm 90^\circ$,

$$\begin{pmatrix} R_Y \\ S_Y \\ W_Y \end{pmatrix}_{\pm 90^\circ} = Y \begin{pmatrix} 0 \\ \pm 1 \\ 0 \end{pmatrix}, \tag{13}$$

and thus similar to drag—apart from the fact that, depending on the sign of β_s, S_Y may either be an along-track acceleration or a deceleration.

For $\beta_s = 0^\circ$, i.e., if the Sun lies in the orbital plane, the constant Y-acceleration becomes:

$$\begin{pmatrix} R_Y \\ S_Y \\ W_Y \end{pmatrix}_{0^\circ} = Y \begin{pmatrix} 0 \\ 0 \\ \frac{\sin(u-u_s)}{|\sin(u-u_s)|} \end{pmatrix}, \tag{14}$$

Note that

$$\frac{\sin(u-u_s)}{|\sin(u-u_s)|} = \begin{cases} +1, & \text{if } 0^\circ < u_s < 180^\circ; \\ -1, & \text{if } 180^\circ < u - u_s < 360^\circ. \end{cases} \tag{15}$$

From Eqs. (14) and (15) we conclude that an OPR Y-term of type $\sim \sin(u - u_s)$ causes an out-of-plane acceleration $W_Y \sim |\sin(u - u_s)|$, which is a superposition of a constant and a twice-per-revolution term.

According to Eqs. (4), (7), and (12), the constant X-component of the SRP model (6) is represented by:

$$\begin{pmatrix} R_X \\ S_X \\ W_X \end{pmatrix} = X \begin{pmatrix} -\sqrt{1-\cos^2\beta_s\,\cos^2(u-u_s)} \\ -\frac{\cos^2\beta_s\,\sin(2u-2u_s)}{2\sqrt{1-\cos^2\beta_s\,\cos^2(u-u_s)}} \\ \frac{\sin 2\beta_s\,\cos(u-u_s)}{2\sqrt{1-\cos^2\beta_s\,\cos^2(u-u_s)}} \end{pmatrix}. \tag{16}$$

The X-bias is a constant acceleration in radial direction for $\beta_s = \pm 90^\circ$:

$$\begin{pmatrix} R_X \\ S_X \\ W_X \end{pmatrix}_{\pm 90^\circ} = X \begin{pmatrix} -1 \\ 0 \\ 0 \end{pmatrix}. \tag{17}$$

In summary we have found that for $\beta_s = \pm 90^\circ$ the constant direct SRP term corresponds to a constant out-of-plane acceleration W_D, the Y-bias to a constant along-track component S_Y, and the X-bias to a constant radial component R_X.

From the results developed in this section it would be easy to calculate the OPR accelerations of the empirical orbit model in the (R,S,W)-directions. We indicated the importance of the result for the OPR term in Y-direction, which may generate a constant out-of-plane component on top of a twice-per-revolution signal. More details are provided in Section 5.1.

3. Solving the perturbation equations for a constant acceleration in W-direction

Osculating satellite orbits are by definition particular solutions of the equations of motion and therefore geocentric. Consequently, it must be possible to obtain the geocenter by intersecting the osculating planes of all satellites included in an analysis. This procedure may be viewed as a purely geometric method to reconstruct the geocenter. It is the guiding principle of our investigation. Specific dynamical conditions have to be met in addition (the geocenter has to lie in the focus of the orbital ellipse) but we do not make use of such conditions in our analysis.

The perturbation equations (Beutler, 2005, Vol I) tell that only a non-vanishing W-component may alter an osculating plane. To explore the correlation between geocenter coordinates and the parameters of the empirical orbit model (5) it is therefore sufficient to study the impact of the W-components of the empirical accelerations (7), (12), (16); the R- and S-components cannot affect the orbital planes. The osculating orbital planes are defined by the right ascension of the ascending node Ω and by the inclination i of the orbits w.r.t. the equatorial plane. The orientation of the osculating ellipses within the plane is given by the argument of perigee ω.

For subsequent use we provide the analytical solution of the perturbation equations for a constant acceleration W in the frame of first-order perturbation theory. The solution becomes particularly simple when approximating the satellite orbits as circles ($e = 0$). In that case the argument of perigee ω can be identified with the node (i.e., $\omega = 0°$) and the perturbation equation for ω may be replaced by one for $u(t)$, the satellite's argument of latitude, because the elements a and e are not altered by a W-acceleration—be it constant or not. The perturbations in u are thus uniquely caused by ω, because $u = \omega + v$, where v is the true anomaly. For circular orbits we may even replace the true anomaly v by the mean anomaly M. With $M = n(t - T_0)$, where n is the mean motion of the satellite and T_0 the node crossing time, we finally get $u = \omega + n(t - T_0)$. Consult Fig. 3 for the definition of the argument of latitude u and the other osculating elements mentioned here.

According to the perturbation equations in the Gaussian form, the modified perturbation equations for the inclination i, the right ascension of the ascending node Ω, and the argument of latitude u read as:

$$\begin{aligned} \frac{di}{dt} &= \frac{W}{na}\cos u, \\ \dot{\Omega} &= \frac{W}{na\sin i}\sin u, \\ \dot{u} &= n - \cos i\,\dot{\Omega}. \end{aligned} \tag{18}$$

First-order perturbation theory asks to consistently use the osculating elements at t_0 on the right-hand sides of Eqs. (18). In order to disencumber the formalism, we use the symbols $i, a, \ldots$ instead of $i_0, a_0, \ldots$ in Eqs. (18) and subsequently, wherever the difference between the perturbed and the osculating elements does not matter, i.e., for the calculation of small quantities (typically perturbations).

The above equations may be solved for a constant out-of-plane acceleration W:

$$\begin{aligned} i(t) &= i_0 + \frac{W}{n^2 a}\sin u(t), \\ \Omega(t) &= \Omega_0 - \frac{W}{n^2 a\sin i}(\cos u(t) - 1), \\ u(t) &= u_0(t) + \frac{W}{n^2 a\tan i}(\cos u(t) - 1), \end{aligned} \tag{19}$$

assuming that the initial epoch $t_0 = T_0 = 0$ corresponds to the satellite's crossing of the ascending node. The argument of latitude of the resulting perturbed orbit was designated with $u(t)$, whereas $u_0(t)$ is related to the osculating elements at t_0. The elements i_0 and Ω_0 are the osculating inclination and the right ascension of the ascending node of the osculating orbit referring to $t_0 = 0$.

The first two of Eqs. (19) tell that the pole of the osculating orbits at times t moves with uniform angular velocity $\dot{u} = n$ on a circle with radius

$$\delta i = \frac{W}{n^2 a} \tag{20}$$

around a fictitious mean pole implicitly defined by the first two of Eqs. (19). Note in particular that the mean pole does not correspond to the pole (i_0, Ω_0) of the osculating orbit at t_0. The coordinates (i_m, Ω_m) of the mean pole may, however, be calculated using the osculating elements at t_0. In the case represented by Eqs. (19) the mean pole is given by:

$$(i_m, \Omega_m) = \left(i_0, \Omega_0 + \frac{W}{n^2 a\sin i}\right). \tag{21}$$

With the mean orbital elements (21) the solution (19) may be brought into the form:

$$\begin{aligned} i(t) &= i_m + \frac{W}{n^2 a}\sin u(t), \\ \Omega(t) &= \Omega_m - \frac{W}{n^2 a\sin i}\cos u(t), \\ u(t) &= u_m(t) + \frac{W}{n^2 a\tan i}\cos u(t), \end{aligned} \tag{22}$$

where obviously

$$u_m(t) = u_0(t) - \frac{W}{n^2 a\tan i}. \tag{23}$$

With Eqs. (22) we introduce a fictitious mean satellite S_m moving on the plane defined by the elements (i_m, Ω_m). As Eq. (23) tells, its motion is synchronous to that of the satellite S_0 moving on the osculating orbit. The constant offset (second term on the right-hand side of Eq. (23)) is due to the difference of the ascending nodes of the fictitious mean and the osculating orbits. The osculating and the fictitious mean satellite, $S_0(t)$ and $S_m(t)$, respectively, lie in good approximation on the same meridian of the fictitious mean orbital plane defined by (i_m, Ω_m) because $i(t) - i_0$ is a small angle. The perturbed satellite $S(t)$ lies on the same meridian, as well. Note that the perturbed, the fictitious mean, and the osculating orbits are all circles, and that the mean (and true) motions in the three orbits are n, i.e., the constant mean motion n of the original osculating orbit. The mean motion is defined by the third of Eqs. (18) and refers to the osculating orbit at time t.

Fig. 4 shows the osculating orbit referring to epoch $t = 0$ (blue), the perturbed orbit (red), and the fictitious mean orbit (black circular border of dark-shaded orbital plane), as well as the corresponding satellites $S_0(t)$, $S(t)$, and $S_m(t)$ at an arbitrarily chosen epoch t. Note that $u(t)$ only might be visualized in Fig. 4 if the osculating orbit referring to epoch t would be drawn, as well. In the interest of clarity we resisted to do that in Fig. 4.

At this point one may wish to consult Appendix A providing a solution of the perturbation equations for a constant W-acceleration in rectangular coordinates (thus bypassing the perturbation equations in the orbital elements) and Appendix B solving the perturbation equations in rectangular coordinates for the term C_{10} (corresponding to the coordinate G_3 of the geocenter).

Let us explicitly state the following important result: The motion of the osculating poles around the fictitious mean pole is synchronous to the motion of the satellite,

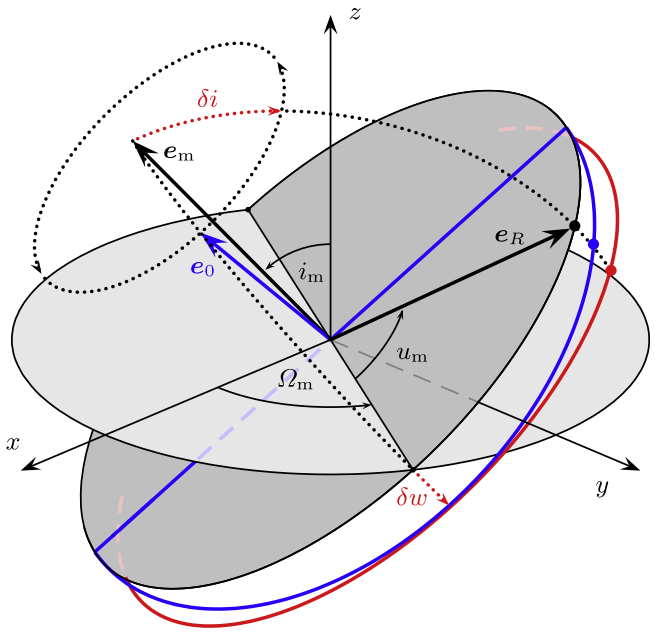

Fig. 4. Perturbed orbit due to a constant out-of-plane acceleration (red), osculating orbit (blue), and mean orbit (black).

which in turn implies that the envelope of all osculating ellipses referring to arbitrary epochs t, i.e., the perturbed orbit, is a circle parallel to the fictitious mean orbit at a distance of

$$\delta w = \frac{W}{n^2} \text{ (in units of meters).} \tag{24}$$

Note that this particular result as well as the values of the mean elements i_m and Ω_m are independent of the location of the osculation epoch. The motion of the satellite within the perturbed orbit is given by the third of Eqs. (19).

The perturbed motion seems to take place in a plane at a distance δw, given by Eq. (24), from the geocenter. Depending on the sign of the acceleration W, the perturbed orbit may lie above or below the mean orbit. Fig. 4 corresponds to a negative value of W, assuming that the Sun is in the hemisphere above the satellite's orbital plane.

According to Eq. (7) there is always a constant acceleration W_D associated with direct SRP—except for $\beta_s = 0°$. For GNSS arcs spanning relatively short time intervals, typically one day, the angle β_s and thus the acceleration $W_D = D \sin \beta_s$ may be assumed as constant (at least for our theoretical studies). A parallel shift of the orbit (represented by the envelope of all osculating orbits) w.r.t. the fictitious mean orbit is always associated with a constant SRP parameter D_0 in the empirical model (6).

It would be easy to generate approximate solutions for the perturbation equations for the W-components of the Y- and X-bias as given by Eqs. (12) and (16). Here we simply state that none but one of these accelerations generate sizeable and constant offsets of the orbital planes. The exception related to the OPR terms of the Y-bias was already mentioned; as we did not include these terms in our analysis, this aspect is not further considered from here onwards (consult, however, Section 5.1).

We build our theory of the correlation between the empirical orbit parameters and G_3 uniquely on Eqs. (7), (19), (20), and (24).

4. Explaining the spurious excursions in the coordinate G_3 of the geocenter

The problem of spurious excursions of the GLONASS-derived G_3 coordinates is discussed for three cases, namely (1) single-satellite solutions when solving for three coordinates of the geocenter referring to the inertial reference frame (in addition to all orbit parameters); (2) single-satellite solutions when only solving for the coordinate G_3 of the geocenter; (3) multi-satellite (multi-plane) solutions when only solving for the coordinate G_3. These cases are dealt with in the first three Sections 4.1–4.3. Section 4.4 contains the key result of our analysis, the representation of the G_3 component of the geocenter as a function of the differences of D_0-values of all satellites from solution series with and without solving for G_3.

4.1. Single-satellite solution estimating three geocenter coordinates

In Section 3 we showed that a constant out-of-plane acceleration W inevitably generates a parallel shift of the resulting perturbed orbit according to Eq. (22). Eq. (7) tells that the direct radiation pressure D_0 always contains a constant out-of-plane component W_D. This is not a problem, because in general the acceleration caused by D_0 also contains non-vanishing components R_D and S_D. A problem shows up, however, as soon as $\beta_s \approx 90°$ and geocenter coordinates are estimated in addition to the parameters D_0 for each satellite of the constellation. The orbit determination problem would become truly singular if

- the GNSS would consist of only one orbital plane,
- the Sun would stand perpendicular above this orbital plane, and if
- all three geocenter coordinates—referring to the inertial coordinate system—were estimated together with the direct SRP parameters.

Under these circumstances the shift of the orbital plane caused by D_0 might be completely absorbed by the three geocenter coordinates without solving for the parameters D_0.

Fig. 5 illustrates the situation: If one solves for a perturbing acceleration W_D normal to the osculating orbital plane, but not for geocenter coordinates, the envelope of the orbital planes would be parallel shifted (from the solid to the dashed orbital plane). According to Eq. (24) the two orbital planes are separated by $\delta w = \frac{W_D}{n^2}$. Obviously, the dashed curve may also be obtained without solving for the parameter W_D, but instead for all three geocenter

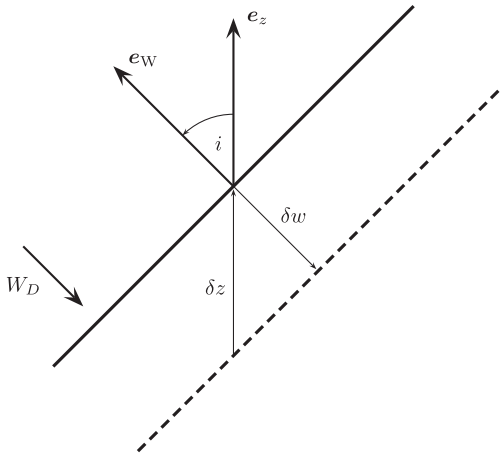

Fig. 5. Shift δz of orbit in e_z-direction caused by a shift δw normal to the orbital plane.

coordinates in the inertial system. The estimated geocenter would be shifted along the orbit normal e_W by a value of δw. Under the assumptions made, we would thus have a true linear dependence between the three inertial geocenter coordinates on one hand and the parameters D_0 related to the orbital plane on the other hand—when making the attempt to solve for both. Consult also Appendix A to explicitly see the relation between the geocenter coordinates and a constant acceleration normal to the orbital plane.

4.2. Single-satellite solution estimating only G_3

In the procedure of the CODE analysis center, in the analysis performed by Meindl (2011), and here, the three estimated coordinates of the geocenter refer to the Earth-fixed system. This fact implies that, unintentionally, coordinate G_3 of the geocenter in the inertial system is estimated, as well, because the transformation between the Earth-fixed and the inertial system consists in essence of a rotation about the e_z-axis leaving all z-coordinates (of station and geocenter vectors) unaffected.

The restricted set of parameters—one instead of three geocenter coordinates—removes the singularity of the generalized orbit determination problem. A strong correlation between the coordinate G_3 and the parameters W_D of the orbital plane may, however, remain: The parameter W_D of the orbit may move the envelope of the shifted plane from the solid to the dashed orbit; a geocenter z-shift of

$$\delta z = \frac{\delta w}{\cos i} \text{ (in units of meters)} \tag{25}$$

can move the orbital plane back to the initial (solid) plane. The procedure is illustrated by Fig. 5.

In order to get more insight into the correlation between the geocenter offset G_3 and the shift in δz caused by the estimation of the SRP parameter D_0, a strap-down simulation was performed in Appendix C. The equatorial coordinates (x, y, z) of an elliptical orbit (for every minute over one day) served as observations to determine the six orbital elements and the parameter D_0 related to a Sun at a constant elevation angle β_s above the orbital plane. The center of the ellipse was shifted by one meter in the z-direction, corresponding to $G_3 = 1$ m in the underlying reference frame.

When ignoring this offset, solving for D_0 (in addition to the six osculating elements), and converting the resulting estimate into an offset δz according to Eqs. (25), (24), (7), one gets an impression of how well formula (25) is met in practice for $\beta_s = 90°$ and how rapidly the approximation deteriorates with β_s decreasing. The second column of Table C.1 shows that the effect is as predicted for $\beta_s = 90°$ and that δz rapidly decreases with decreasing β_s. The third column of Table C.1 stems from a parameter estimation including the six orbital elements, D_0 *and* G_3. A very high degree of correlation results for $\beta_s = 90°$, which is rapidly reduced with a decreasing angle β_s. The last column of Table C.1 shows that biases remain in the system if only the six orbital elements and the parameter D_0 are estimated: For a perfect a priori model the root-mean-square (RMS) value a posteriori should be close to zero (error-free observations assumed). The RMS varies between 15 cm for $\beta_s = 90°$ to about 36 cm for $\beta_s = 0°$. The simulation is a very coarse approximation of the actual problem but reveals the key characteristics of the original problem.

4.3. Multi-satellite/plane solution estimating only G_3

In reality we do not only have one, but three or six orbital planes in the cases of GLONASS and GPS, respectively. The additional orbital planes in principle remove the singularity problem discussed above. The correlation between parameters D_0 and G_3 in the single-satellite case tell, however, that the observations of the satellites in the original plane cannot contribute (much) to the determination of G_3. With only slight exaggeration we may therefore state that G_3 is determined with the observations of only two orbital planes for GLONASS when $\beta_s \approx 90°$ for one plane. Fig. 6 illustrates the situation with three orbital planes (to be interpreted either as building blocks of the GPS or as the complete GLONASS). The e_z-axis points to the North pole.

The six orbital planes of the GPS are evenly spaced by 60° (in the equatorial plane) and labeled by A, B, ..., F. Only the planes A, C, and E and their normal vectors e_A, e_C, and e_E are provided in Fig. 6. In the case of the GPS, with an inclination $i \approx 55°$ and a separation of planes A, C, and E of 120° in the equator, the three orbital planes are mutually orthogonal—and so are the orbit normal vectors. The three planes may thus be interpreted as the three faces of a cube intersecting in one of its vertices. The e_z-axis, pointing to the North pole, corresponds to the (continuation of the) space diagonal of this cube. Note that the normal vector of one of the orbital planes is the intersection of the other two orbital planes.

For the GPS the weakening of the G_3 solution, e.g., due to a large angle β_s over plane A, is mitigated by the three

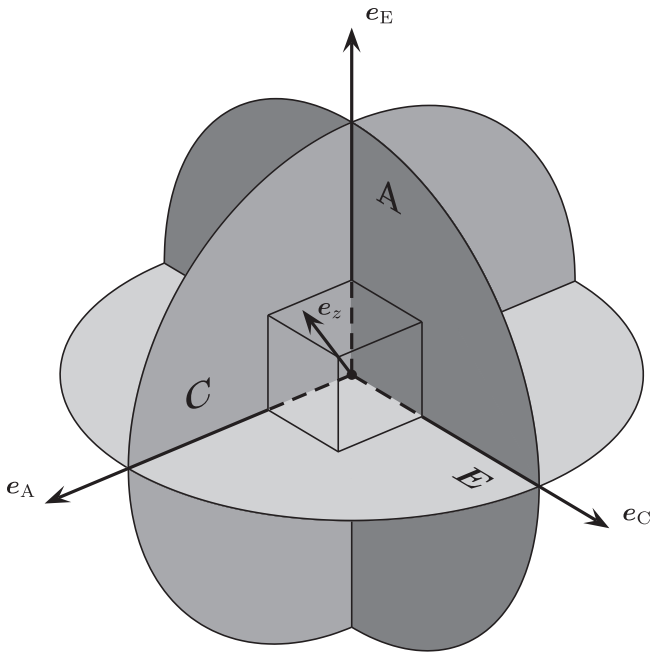

Fig. 6. Orbital planes A, C, and E of the GPS and the corresponding orbit normal vectors; unit vector $\boldsymbol{e}_z$ points to the North pole.

planes B, D, and F. If plane A has a quasi-singularity with a large β_s, all other planes, in particular B, D, and F, have rather small angles β_s. These facts explain why G_3 is well determined with the GPS when using the CODE empirical SRP model (5), (6)—even when $\beta_s \approx 80^\circ$ for one of the orbital planes.

In the case of GLONASS with inclinations of $i \approx 65^\circ$, Fig. 6 has to be used with some caution: The three GLONASS planes are not mutually orthogonal, neither are the corresponding orbit normal vectors. Therefore, the orbit normal of one plane does not lie in the other two orbital planes. The inclination angles of the orbit normal vector of one plane w.r.t. the two other planes remain, however, small.

The Galileo system will be similar to GLONASS by having only three orbital planes. It will be similar to the GPS by having an inclination of about 55°. Galileo is thus well described by Fig. 6.

4.4. The geocenter shift G_3 as a function of D_0-differences

Is it possible to relate the estimated geocenter offset G_3 to the differences of the D_0-estimates for all satellites in the solution series with and without the estimation of G_3? To answer this question we perform a thought experiment, assuming that (a) the observations of a three-plane GNSS are uniquely contaminated by small normally distributed random errors; and (b) that the a priori model of the observations is perfect, apart from a sizeable geocenter offset G_3. The outcome of the experiment will be the following:

- The solution series including the estimation of G_3 will provide the correct values for all D_0 and for G_3 (somewhat weakened because one orbital plane is not contributing to this estimate).
- The solution series which does not include the estimation of G_3 will contain systematic errors. This implies in particular that the estimates of D_0 will be biased. The biases will be large for those satellites having large angles β_s. Appendix C gives more details.

Based on this thought experiment and based on the discussion of a GNSS with only one satellite (orbital plane) earlier on in this section, we postulate that the estimate of the geocenter coordinate G_3 must be explained by the differences of the direct SRP parameters in both solution series: Let D and D' be the direct SRP parameter estimates for a particular orbital plane from a solution including the estimation of G_3 and keeping this estimate constrained to zero, respectively. Assuming satellites of the same type (surface properties, mass, attitude control) within the orbital plane, the best values for the parameters D and D' are the mean values over all s satellites in the plane:

$$D = \frac{1}{s}\sum_{k=1}^{s} D_k \quad \text{and} \quad D' = \frac{1}{s}\sum_{k=1}^{s} D'_k, \tag{26}$$

where the D_k and D'_k are the constant direct SRP parameters associated with the satellite k of the plane.

According to Eq. (7), the difference

$$\Delta D \stackrel{\text{def}}{=} D - D' \tag{27}$$

generates a constant acceleration $\Delta W = \Delta D \sin\beta_s$. By virtue of Eq. (24) this constant acceleration causes an orbit displacement of $\delta w = \Delta D \sin\beta_s / n^2$ normal to the orbital plane, where n stands for the mean motion of the satellites. The orbital plane is thus shifted in the z-direction by $\delta z = \delta w / \cos i = \Delta D \sin\beta_s / (n^2 \cos i)$. The total theoretical shift δz of the geocenter induced by the plane-specific ΔD_ℓ values, $\ell = 1, 2, \ldots, p$, of all p orbital planes, thus simply is:

$$\delta z = \frac{\sum_{\ell=1}^{p} \Delta D_\ell \sin\beta_{s\ell}}{n^2 \cos i}, \tag{28}$$

where the mean motion n as well as the inclination i are assumed to be the same for all satellites of the system. The angle $\beta_{s\ell}$ is assumed to be the same for all satellites of plane ℓ. Our hypothesis, namely that the estimate of coordinate G_3 compensates δz, implies that we should have

$$\delta z + G_3 \approx 0. \tag{29}$$

Fig. 7 shows that our hypothesis is approximately true for the GLONASS system. The red and the black curves correspond to the estimated G_3-values and to the values $-\delta z$, where δz was calculated according to Eq. (28). The black curve in Fig. 7 (bottom) shows $\delta z + G_3$, which we suspected to be close to zero. The signal is not exactly zero, but it has greatly reduced amplitudes when compared to either G_3 or δz.

Fig. 8 provides the individual constituents of δz in Eq. (28) related to the three GLONASS orbital planes. The

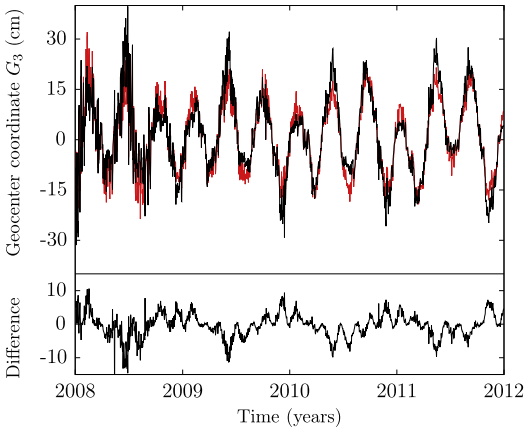

Fig. 7. Coordinate G_3 from GLONASS: estimated (red) and reconstructed (black) from ΔD-components according to Eq. (28); bottom: difference.

resulting total signal near the maxima and minima is in most cases dominated by exactly one contributing orbital plane. This fact indicates that one needs at least three orbital planes without near-singularities when trying to determine G_3 with a particular GNSS.

So far, we only considered GLONASS arcs of one day for the creation of the geocenter time series. One may suspect that longer arcs would reduce the artifacts in Fig. 7. Fig. 9, showing the time series of G_3-estimates based on one-day and (overlapping) three- and seven-day arcs, indicates that the arc length is an important aspect for geocenter determination. The three-day arcs (red curve) result in moderately reduced excursions. The seven-day arcs (green) significantly reduce the excursions, particularly those caused by the plane with the maximum β_s-values. Seven-day arcs correspond to the length of SLR arcs (see Section 5.2). Longer arcs would thus be recommendable for geocenter determination. For other parameters, in particular for orbit parameters and station coordinates, one- or three-day arcs are clearly preferable, because currently our GLONASS orbit models are not sufficient to generate longer than three-day arcs with only few parameters. Systematic errors in the orbits and other parameters would result. The CODE final products are, e.g., based on

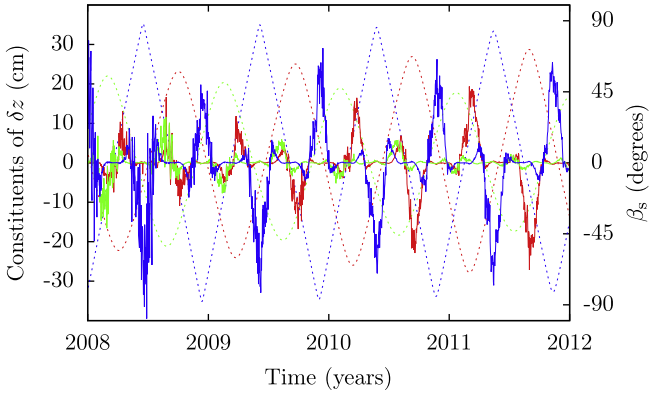

Fig. 8. Plane-specific constituents of δz (solid) and corresponding angles β_s (dashed) for GLONASS.

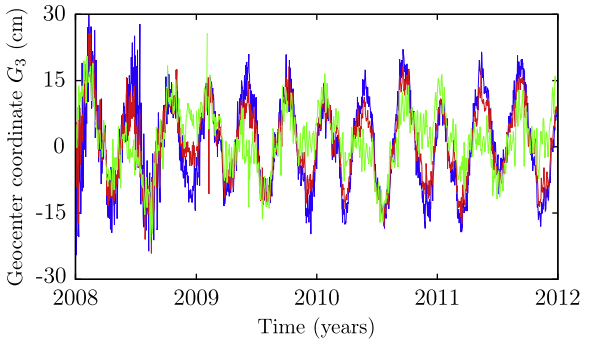

Fig. 9. Coordinates G_3 from GLONASS using one-day arcs (blue), three-day arcs (red), and seven-day arcs (green).

three-day arcs, which is a well established practice since more than twenty years.

Let us now apply Eq. (28) to the GPS time series of geocenter estimates. A first inspection of the coordinates G_3 determined with the GPS in Fig. 1 of Section 1.4 did not reveal a strong correlation of the geocenter time series with the angles β_s of the individual orbital planes. Fig. 10 corresponds to Fig. 7, but compares G_3-estimates and δz-values based on GPS observations. Formula (28) predicts the behavior of G_3 even much better than in the case of GLONASS and the sum $\delta z + G_3$ (Fig. 10, bottom) differs from zero only by fractions of one centimeter. Our theory therefore may be applied to both fully deployed GNSS.

5. Geocenter determination using a generalized empirical orbit model

5.1. GNSS-derived geocenter coordinates

The article (Thaller et al., in press) has the focus on the combination of GNSS- and SLR-observations for the estimation of the geocenter. The solutions of the GNSS-related NEQs were artificially weakened by solving not only for the OPR parameters associated with $\boldsymbol{e}_X$, but for

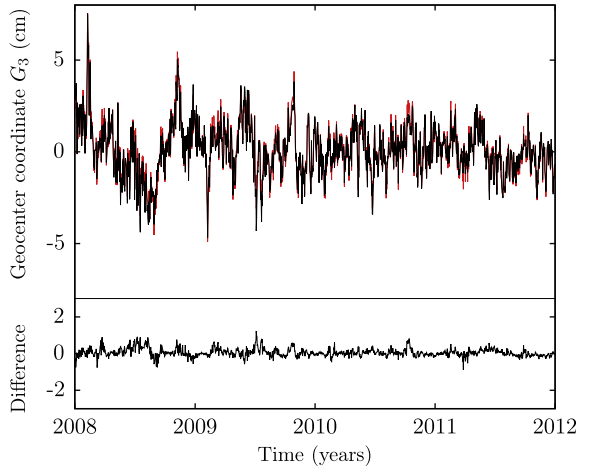

Fig. 10. Coordinate G_3 from GPS: estimated (red) and reconstructed (black) from ΔD-components according to Eq. (28); bottom: difference.

all three directions $\boldsymbol{e}_D$, $\boldsymbol{e}_Y$, and $\boldsymbol{e}_X$ (in addition to the three constant components) in the empirical model (5), (6). As a consequence the GNSS-only estimates of the coordinate G_3 became really bad with excursions up to ± 15 cm. Adding the SLR observations to LAGEOS subsequently greatly improved the bad solutions.

In view of the theory developed in the previous sections it seems clear that the OPR parameters in the $\boldsymbol{e}_D$-direction (see Eq. (7)) cannot be guilty for the massive quality loss. In order to clarify this aspect we generated two more solution series with the GPS data used in our analysis, one including the OPR estimates along $\boldsymbol{e}_D$, one including the OPR estimates along $\boldsymbol{e}_Y$—both times in addition to the parameters of the standard CODE model. Fig. 11 confirms our theory: The OPR terms along $\boldsymbol{e}_D$ have virtually no impact on the geocenter. The impact of adding the OPR terms along $\boldsymbol{e}_Y$, on the other hand, is absolutely devastating.

How can this effect be explained despite the fact that we have six orbital planes in the GPS? Eqs. (12) and (14) answer this question: As mentioned, the OPR terms along $\boldsymbol{e}_Y$ are indeed able to generate a constant W-acceleration (actually a non-zero mean in W-direction) for $\beta_s = 0°$. As opposed to the effects caused by a constant acceleration D_0, where the maximum angle β_s was limited by Eq. (10) for the GPS, the case $\beta_s = 0°$ occurs twice per (draconitic) year for each orbital plane. The estimation of the OPR parameters in $\boldsymbol{e}_Y$ is insofar worse than the estimation of constant parameters in $\boldsymbol{e}_D$, because if there is a small angle β_s associated with, e.g., plane A, β_s is also small for plane D. The same is true for the other pairs of orbital planes separated by 180° in the equator. For orbital planes with $\Omega = 0°$ and $\Omega = 180°$ the cases where $\beta_s = 0°$ even occur simultaneously. The geometry is illustrated by Fig. 12, where the angles β_s of the planes separated by 180° in the equator have the same line style.

The curves with the same line style all intersect at $|\beta_s| < 15°$ (shaded area in Fig. 12), i.e., at small angles. We may therefore say with only slight exaggeration that we have critical situations with small angles β_s simultaneously in two orbital planes separated by 180° in the equator about every two months. The situation is particularly pronounced for the orbital planes with $\Omega \approx 0°$ and $\Omega \approx 180°$ (dotted curves in Fig. 12).

As quasi-singularities occur simultaneously in the two building blocks A/C/E and B/D/F of the GPS (see Fig. 6), the GPS can no longer profit from its six orbital planes—two of them may be disregarded for $\beta_s \approx 0°$ due to the parametrization used in this section.

5.2. SLR-derived geocenter coordinates

SLR solutions based on spherical satellites are known to be very well suited for geocenter estimation (see Section 1.1). As we were successfully producing bad GNSS-derived estimates of G_3 by generalizing our empirical SRP model (5), the question arose whether the SLR-derived estimates of G_3 are sensitive to similar changes in the SRP model. The LAGEOS data 2008–2010 from Thaller et al. (in press) were re-analyzed for that purpose and different solutions were generated with different sets of empirical accelerations estimated per 7-day arc:

- a constant along-track acceleration S_0,
- S_0 and a constant direct acceleration D_0,
- S_0 and a constant out-of-plane acceleration W_0.

Once-per-revolution parameters in along-track $\boldsymbol{e}_S$- and out-of-plane $\boldsymbol{e}_W$-directions were estimated in addition in all three solution types. The first solution type represents our standard SLR solution, which may serve as reference. The resulting coordinates G_3 of the geocenter are shown in Fig. 13. The estimation of an additional acceleration D_0 for the direction $\boldsymbol{e}_D$ to the Sun obviously has almost no impact on the estimated geocenter coordinates. The estimation of an acceleration W_0 in the out-of-plane direction $\boldsymbol{e}_W$, however, clearly weakens the SLR-derived geocenter estimates. The blue curve therefore shows what might happen for the SLR solution in the worst case.

The insensitivity of the geocenter w.r.t. the parameter D_0 may be explained with the angles β_s for the two LAGEOS satellites (see Fig. 14): The maximum β_s for LAGEOS-2 is 76° and in most cases $|\beta_s| < 40°$; a maximum of $|\beta_s| \approx 90°$

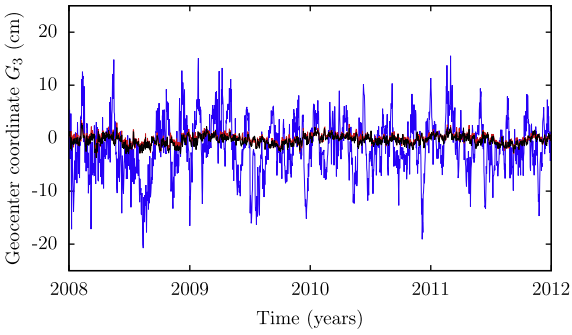

Fig. 11. Coordinate G_3 from GPS using the CODE orbit model (black), the CODE model plus the OPR terms along $\boldsymbol{e}_D$ (red), and the CODE model plus the OPR terms along $\boldsymbol{e}_Y$ (blue).

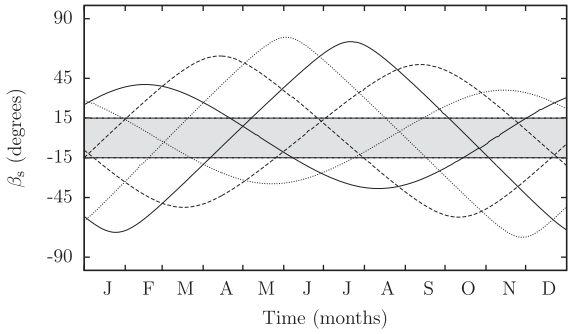

Fig. 12. Angles β_s of the GPS constellation (same line style for planes separated by 180° in the equator).

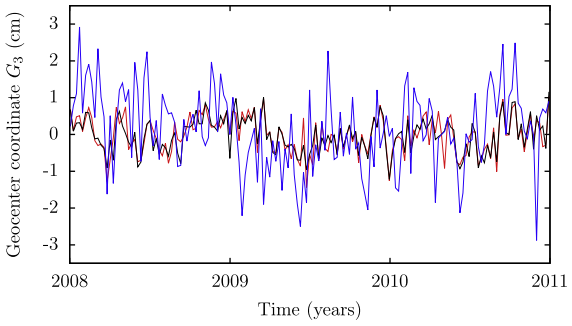

Fig. 13. Coordinate G_3 estimated by SLR with empirical accelerations S_0 (black), S_0 and D_0 (red), S_0 and W_0 (blue).

is possible for LAGEOS-1, but this is counterbalanced by LAGEOS-2.

The D_0-estimates (corrections w.r.t. the a priori value) are below $0.5 \cdot 10^{-9}$ m/s^2 for LAGEOS-2. If we apply Eq. (28) for the maximum angle $\beta_s = 76°$, we obtain a maximum theoretical effect on the geocenter of only $\delta z = 3.6$ mm. The D_0-estimates are usually below $1.0 \cdot 10^{-9}$ m/s^2 for LAGEOS-1, resulting in a maximum theoretical effect of $\delta z = 13.6$ mm for $\beta_s = 90°$.

If we compute a single-satellite solution based only on LAGEOS-1 (with estimating D_0), the variations in the geocenter are negligible except for periods when $|\beta_s|$ reaches its maximum values. During these time spans, the impact on the component G_3 of the geocenter may reach about 2 cm, confirming the theoretical value derived above. In the case of a LAGEOS-2 solution, the variations in the geocenter series are negligible (always below 1 mm), confirming the theoretical value derived above, as well.

The third reason for the insensitivity of the geocenter w.r.t. the estimation of D_0-parameters resides in the length of the LAGEOS orbital arcs (i.e., 7 days), which also implies a significant change of the angles β_s during this time span. Fig. 14 (bottom) shows that β_s varies within one week by up to 5° and 10° for LAGEOS-1 and LAGEOS-2, respectively. This range of values de-correlates the relationship between a constant ΔD and δz in Eq. (28). The angles β_s for the GNSS satellites change within one orbital arc (one day) by about 1°, only. A simulation based on the method outlined in Appendix C, but with a Sun moving with 1°/day in the ecliptic, revealed, as well, that the arc length plays a key role: The correlation rapidly decreases when the arc length increases.

As the angle β_s does not matter for the relationship between a constant acceleration in W-direction and the geocenter (cf. Eqs. (24) and (25)), we see an impact on the geocenter series when estimating a W_0-parameter (Fig. 13). The differences are up to about 2 cm. But thanks to the mean motion n of the satellite in Eq. (24), the differences are much smaller for the LAGEOS satellites than for the GNSS satellites.

From these experiments we conclude that the LAGEOS-based geocenter solutions greatly benefit from the orbit characteristics resulting in an insensitivity w.r.t. the estimation of D_0-parameters, and only a small sensitivity w.r.t. a W_0-parameter. In addition, the SRP is much better known for the LAGEOS satellites than for the GNSS satellites, which is why D_0 usually needs not to be estimated. Together with the theoretical considerations concerning the SLR and GNSS observation types given in Section 1.1, the experiments in this section clearly show the superiority of SLR compared to GNSS for the estimation of meaningful geocenter series.

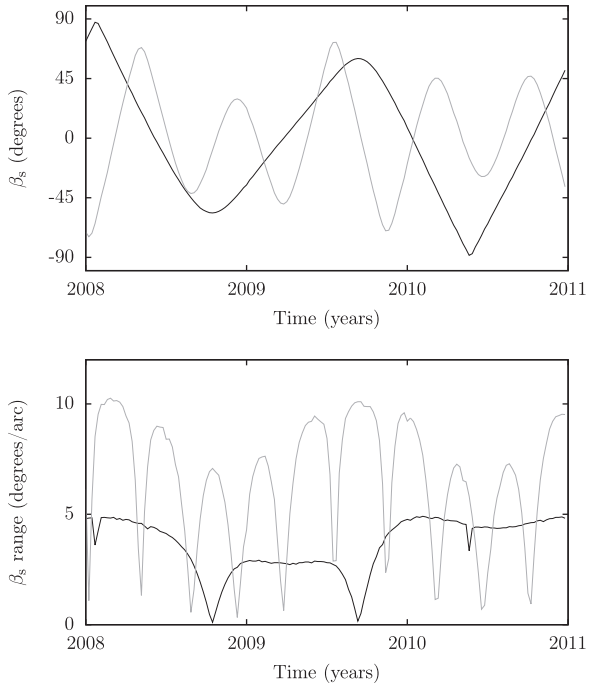

Fig. 14. Top: elevation β_s of the Sun above/below the orbital planes of the LAGEOS-1 (black) and LAGEOS-2 (gray) satellites; bottom: range of β_s within each 7-day arc.

6. Summary and conclusions

Our investigations were motivated by Fig. 1 (bottom) showing the estimates of the coordinate G_3 of the geocenter and the elevation angles β_s of the Sun above or below the three GLONASS orbital planes. The correlation of G_3 with β_s is so obvious that a detailed analysis of the correlations between G_3 and the orbit parameters seemed appropriate.

For this purpose the constant constituents of the SRP model (5), (6) were decomposed into (R,S,W)-components (radial, along-track, out-of-plane) in Section 2.2. We found that the acceleration associated with the parameter D_0 in Eq. (6) gives rise to a constant W-component (assuming β_s as constant over the arc length). We found furthermore that for $|\beta_s| = 90°$ the R- and S-components related to the parameter D_0 are zero (see Eq. (8)) and that, according to Eq. (11), the Sun regularly almost assumes this elevation for GLONASS. According to Eq. (10) the maximum elevation of the Sun above the GPS planes is about 78.5°, implying that even for the maximum β_s-angles there are still

sizeable R- and S-components associated with direct radiation pressure, which helps de-correlating the geocenter coordinate G_3 and the SRP parameters D_0 for GPS. It is important to note that only a constant D-component and an OPR component in Y are capable of generating non-zero mean values in the W-component over one revolution.

In Section 3 the essential results of first-order perturbation theory were put together. This theory says that a constant perturbation normal to an orbital plane causes the perturbed orbit seemingly to lie in a plane which does not contain the geocenter. The distance of the geocenter from the perturbed orbital plane is given by Eq. (24). The geometry of the perturbation is illustrated by Fig. 4.

In Section 4 we first studied a hypothetical GNSS with only one orbital plane and assumed a constant perturbing acceleration perpendicular to this plane (Sun normal to the orbital plane). The orbit determination problem becomes singular, if the parameter D_0 and the three geocenter coordinates in the inertial system are determined in the same parameter estimation procedure. If only the inertial component G_3 of the geocenter is estimated in addition to D_0, a high correlation remains between the parameters G_3 and D_0.

If two orbital planes are added to the one-plane-GNSS (for which $|\beta_s| \approx 90°$) in such a way that the three planes are separated by 120° in the equator, the determination of the geocenter remains weak.

The total shift of the geocenter due to the differences of the constant parameters D_0 in the solutions without and with the estimation of G_3, respectively, is given by Eq. (28), which may be viewed as the core result of our work. The equation predicts the geocenter offsets almost perfectly for the GPS and rather accurately for the GLONASS (see Figs. 10 and 7).

A comparison of Figs. 7 and 10 clearly tells that the GLONASS-derived coordinates G_3 are artifacts. What is the nature of the excursions in the GPS-derived geocenter as shown in Fig. 10? From the fact that Eq. (28) perfectly describes the excursions in terms of the differences (27) we are not allowed to conclude that the excursions in Fig. 10 are artifacts: We might have started our investigation from an arbitrarily chosen origin of the terrestrial network (e.g., offset by one meter w.r.t. the ITRF origin), in which case the estimated components G_3 of the geocenter would have removed this wrong value. But formula (28) still would describe the estimated coordinates G_3 correctly as a function of the values (27). This is why a discussion of the nature of the GPS-derived geocenter variations would have to involve the SLR time series as reference. We decided not to conduct such an investigation here, because our GPS-derived geocenter time series is based on a global network of only 92 combined GPS/GLONASS receivers and not on the much larger network of GPS receivers used, e.g., by the CODE or other IGS analysis centers.

Section 5.1 tells that the orbit parametrization plays a key role when studying artifacts in the components G_3 of the geocenter. When adding the two OPR parameters associated with the Y-component of the empirical SRP model (6) to the standard model used in the previous sections, the quality of the GPS-derived coordinates G_3 breaks down completely. The artifacts are almost as bad as for the GLONASS-derived results (see Fig. 11). The reason for this behavior was clearly identified: For $\beta_s \approx 0°$ the SRP model contains a non-zero mean W-component caused by the two OPR terms in Y.

Having said that orbit parametrization plays an important role one might conclude that the problems encountered in this article are uniquely caused by the CODE orbit model (5), (6). This is not true, however: Alternative models, like, e.g., box-wing models, cannot live without model parameters, which have to be determined in the parameter estimation process. Our theory asks that each empirical acceleration standing behind such a free parameter has to be decomposed into the (R,S,W)-components—along the lines presented in Section 2.2. As soon as W-components with non-zero means over a revolution result, there is the danger of generating artifacts.

In Section 5.2 we checked whether our theory also applies to geocenter series determined with SLR. The question can by answered by "yes, but ...": When adding a constant acceleration in $\boldsymbol{e}_W$ (and estimating the associated parameter W_0), the SLR solutions are considerably weakened (blue curve in Fig. 13), but not to the same extent as the GLONASS solutions (see Fig. 7). One might have expected a much stronger degradation of the SLR solutions, because they are based only on two satellites. The blue curve is a worst case scenario for LAGEOS, showing what would happen when solving for a constant out-of-plane acceleration for each arc. In the assumptions underlying our theory (β_s assumed constant over the arc length) the solution when solving for a constant D_0 (red curve) should be the same as the blue curves if $\beta_s = 90°$. The fact that this is not the case indicates that the change of the angle β_s within the arc plays an important role. The results of Section 5.2 confirm that SLR, applied to the geodetic LAGEOS satellites, is an excellent tool to determine geodetic datum parameters like the geocenter.

One might believe that a GNSS with satellites equipped with 3-D accelerometers, measuring the surface accelerations along three spacecraft-fixed axes, would remove the problem associated with the SRP models. This actually would be true for accelerometers with infinite bandwidth. Unfortunately, such devices do not exist, implying that at the minimum one offset parameter has to be determined per accelerometer component in the analysis. For $|\beta_s| = 90°$ this is equivalent to determining a constant acceleration along $\boldsymbol{e}_W$ (and two other accelerations)—so we are back to where we started. Let us point out, however, that accelerometry on GNSS satellites would be very useful, because it would take care of all the time-varying aspects of solar radiation pressure. It is, however, also clear that it would not resolve all problems.

Let us conclude with a few remarks about the future, in particular about Galileo. This system will be based on only

three orbital planes like GLONASS. One therefore might expect a rather bad performance for the determination of the geocenter component G_3. The inclinations of the Galileo orbits will, however, be essentially the same as those of the GPS, implying that the maximum angle β_s is below 80°, which greatly reduces the correlation between the parameters D_0 and G_3. We therefore predict that the coordinates G_3 estimated with Galileo will have a signature like those in Fig. 7, but with substantially reduced amplitudes.

From the perspective of geocenter determination we would advocate a hypothetical GNSS with, let us say, 30 satellites with only one satellite per equally spaced orbital plane. The separation of the orbital planes would then be 12° in the equator. This system design would result in a much better sampling of the SRP parameters as a function of β_s at each point in time. Such a GNSS would be much less prone to the kind of quasi-singularities as discussed in this work.

Acknowledgments

We would like to thank our partners in the CODE consortium: The Federal Office of Topography (swisstopo, Wabern, Switzerland); the Institut für Astronomische und Physikalische Geodäsie, Technische Universität München (IAPG/TUM, Germany); and the Bundesamt für Kartographie und Geodäsie (BKG, Frankfurt a. M., Germany) for the fruitful collaboration going far beyond financial support in the framework of CODE.

We also would like to thank the three reviewers and the editor of this article. Their comments were extremely helpful to polish the original manuscript.

Appendix A. Solving the perturbation equations for W in Cartesian coordinates

In their original form, the perturbation equations including the $1/r$-potential and an acceleration W normal to the unperturbed orbital plane read as:

$$\ddot{\boldsymbol{r}} = -GM\,\frac{\boldsymbol{r}}{r^3} + W\,\boldsymbol{e}_W. \tag{A.1}$$

Note that $W = D_0$ for $\beta_s = 90°$ (see Eq. (8)). One therefore may view this appendix also as a treatment of direct solar radiation pressure if the Sun is perpendicular above the orbital plane.

Let us now assume that the unperturbed orbit is circular with radius $r = a$. Eq. (A.1) may then be brought into the form

$$\ddot{\boldsymbol{r}} = -GM\,\frac{\boldsymbol{r} - Wa^3/(GM)\,\boldsymbol{e}_W}{r^3} = -GM\,\frac{\boldsymbol{r} - W/n^2\,\boldsymbol{e}_W}{r^3}. \tag{A.2}$$

Performing the transformation

$$\boldsymbol{r}' \overset{\text{def}}{=} \boldsymbol{r} - W/n^2\,\boldsymbol{e}_W \tag{A.3}$$

in Eq. (A.2) leads to the equations of motion

$$\ddot{\boldsymbol{r}}' = -GM\,\frac{\boldsymbol{r}'}{r'^3}. \tag{A.4}$$

Eq. (A.4) says that the satellite moves on a Keplerian orbit with the unperturbed semi-major axis, with center $W/n^2\,\boldsymbol{e}_W$, and with the orbital plane parallel to the original plane. We made use of the fact that the mean motion n of the satellite is not affected by a force normal to the orbital plane and that $r' \approx r$.

The latter relation does not hold strictly in the mathematical sense, because

$$\begin{aligned} r' &= \sqrt{r^2 + \frac{W^2}{n^4}} \approx r\left(1 + \frac{1}{2}\frac{W^2}{n^4 a^2}\right) \\ &\approx r\left(1 + 1.3 \cdot 10^{-14}\right), \end{aligned} \tag{A.5}$$

where we used typical values W, a, and n for a GPS satellite. The approximation is thus certainly allowed—at least for the arc lengths we have to deal with.

Appendix B. Solving the perturbation equations for C_{10} in Cartesian coordinates

It is well known that the terms C_{10}, C_{11}, and S_{11} of the development of the Earth's gravity potential into spherical harmonics are related to the coordinates (G_1, G_2, G_3) of the Earth's center of mass through the equations (see Beutler, 2005, Vol. I):

$$C_{10} = \frac{G_3}{a_e}, \quad C_{11} = \frac{G_1}{a_e}, \quad S_{11} = \frac{G_2}{a_e}, \tag{B.1}$$

where a_e is the equatorial radius of the Earth. Instead of solving for a common offset of the network of observing sites, it is thus also possible to solve for the first-degree coefficients of the spherical harmonics expansion. The perturbation equations for C_{10} read:

$$\ddot{\boldsymbol{r}} = -GM\,\frac{\boldsymbol{r}}{r^3} + \nabla V_{10}, \tag{B.2}$$

where

$$V_{10}(r, \phi) = C_{10}\,\frac{GMa_e}{r^2}\,\mathrm{P}_1^0(\sin\phi) \tag{B.3}$$

and where ϕ is the latitude of the satellite. The Legendre polynomial of first degree is given by:

$$\mathrm{P}_1^0(\xi) = \frac{1}{2}\frac{\mathrm{d}}{\mathrm{d}\xi}\left(\xi^2 - 1\right) = \xi. \tag{B.4}$$

As $\xi = \sin\phi = \frac{z}{r}$, the geopotential term (B.3) may be written as:

$$V_{10}(r, z) = C_{10}\,GMa_e\,\frac{z}{r^3}. \tag{B.5}$$

Note that $r = r(x, y, z)$. From the above equation we obtain the perturbing force as

$$\nabla V_{10} = C_{10}\, GMa_e \nabla\left\{\frac{z}{r^3}\right\} = C_{10}\, GMa_e \begin{pmatrix} -3\frac{xz}{r^5} \\ -3\frac{yz}{r^5} \\ -3\frac{z^2}{r^5}+\frac{1}{r^3} \end{pmatrix}. \quad \text{(B.6)}$$

After some algebra one obtains the representation of this gradient in the (R,S,W)-system as

$$\nabla V_{10} = C_{10}\, \frac{GMa_e}{r^3} \begin{pmatrix} -2\sin i \sin u \\ +\sin i \cos u \\ \cos i \end{pmatrix}. \quad \text{(B.7)}$$

Let us now introduce this representation into the equations of motion (B.2). Without loss of generality we may interpret this equation as a coordinate equation with the plane of the unperturbed orbit as fundamental coordinate plane (we thus have $i = 0°$), which results in:

$$\ddot{\boldsymbol{r}} = -GM\,\frac{\boldsymbol{r}}{r^3} + \frac{GM\, a_e\, C_{10}}{r^3}\, \boldsymbol{e}_W. \quad \text{(B.8)}$$

Using $G_3 = a_e C_{10}$ from Eq. (B.1) we may write

$$\ddot{\boldsymbol{r}} = -GM\,\frac{\boldsymbol{r} - G_3\, \boldsymbol{e}_W}{r^3}. \quad \text{(B.9)}$$

Note that Eq. (B.9) is the same as (A.2) (apart from the pre-factor of vector $\boldsymbol{e}_W$). There is one subtle difference: Thanks to the pre-factor $1/r^3$ in (B.7) the above equation does not only hold for circular orbits, but for any eccentricity e. Proceeding in the analogous way as in Appendix A and performing the substitution

$$\boldsymbol{r}' \stackrel{\text{def}}{=} \boldsymbol{r} - G_3\, \boldsymbol{e}_W \quad \text{(B.10)}$$

in Eq. (B.9) finally leads to the equations of motion

$$\ddot{\boldsymbol{r}}' = -GM\,\frac{\boldsymbol{r}'}{r'^3}. \quad \text{(B.11)}$$

Our conclusions are analogous to those of Appendix A: Eq. (B.11) says that the satellite moves on a Keplerian orbit with the unperturbed semi-major axis a, with center $G_3\, \boldsymbol{e}_W$, and with the orbital plane parallel to the original plane. Again we used $r \approx r'$, knowing already that this approximation is no issue, in practice.

Comparing Eqs. (A.4) and (B.11) we may conclude that for circular orbits there is a correlation of 100% between the parameter D_0 for $|\beta_s| = 90°$ and the estimation of the three geocenter offsets in the inertial system!

Appendix C. A parameter estimation based on simulated observations

The correlation between the geocenter coordinate G_3 and the direct radiation pressure parameter D_0 may be illustrated by a simple parameter estimation problem preserving, however, the key features of the original one. Its characteristics are:

- The Cartesian coordinates of the position vector of a GPS-like satellite are used as observations. One day worth of error-free observations, separated by one minute, is assumed.
- The orbit of the satellite solves the two-body problem. Its origin is, however, not in the origin of the selected coordinate system, but shifted in z-direction by $G_3 = +1\,\text{m}$.
- The orbit is reconstructed for $\beta_s = 0°, 10°, \ldots, 90°$. The G_3-offset of one meter is ignored; instead a SRP coefficient D_0 is solved for together with the six osculating elements. The unit vector $\boldsymbol{e}_D$ was assumed to lie in the plane defined by the z-axis of the coordinate system and the orbit normal vector. The partial derivatives w.r.t. D_0 are obtained by numerical integration; the a priori orbit and its partial derivatives w.r.t. to the osculating elements are obtained analytically based on the formulas of the two-body problem. There are seven parameters in the adjustment.
- In order to study the correlation between G_3 and D_0 an additional eight-parameter adjustment is performed, where both, D_0 and G_3 are determined.

The results may be found in Table C.1: Column 1 contains the elevation β_s of the Sun above the orbital plane; column 2 the offsets δz derived from the estimated D_0 using Eq. (28); column 3 the correlation coefficient κ of the parameters G_3 and D_0 from the eight-parameter adjustment; and column 4 the root-mean-square (RMS) errors a posteriori of the observations calculated using the standard formulas of the adjustment.

The first line of Table C.1 shows that the parameter D_0 cannot absorb any fraction of the geocenter offsset G_3 if the Sun lies in the orbital plane. This is underlined by the correlation coefficient $\kappa \approx 0\%$. The RMS error a posteriori is about a third of the offset. The case $\beta_s = 0°$ also corresponds to an adjustment solving only for the six osculating orbit elements. An inspection of the residuals (not provided here) shows a clear systematic behavior with an once-per-revolution signature.

The last line shows that the entire effect of 1 m can be absorbed by D_0 for $\beta_s = 90°$. The correlation coefficient $\kappa \approx -91\%$ indicates that the two critical parameters are almost linearly dependent.

The other lines of Table C.1 show that the correlation and the fraction of the offset absorbed by D_0 rapidly decrease from $\beta_s = 90°$ to $\beta_s = 0°$. For GNSS constellations one may safely state that a geocenter offset induced by D_0 is dominated by the orbital plane with the largest $|\beta_s|$.

What would happen in a multi-satellite adjustment involving $s > 1$ satellites with different angles β_s (and different vectors $\boldsymbol{e}_D$)? Based on the simulation documented by Table C.1 we give the following answers:

- An adjustment keeping the geocenter fixed at the wrong position will result in exactly the same D_0-estimates for every satellite as in the single-satellite adjustments,

Table C.1
Results of the adjustments.

β_s in degrees	δz in mm	κ in %	RMS in mm
0	0	−1.5	363
10	1	−3.6	363
20	3	−5.7	363
30	6	−8.2	362
40	13	−11.1	361
50	25	−15.1	359
60	49	−21.0	355
70	113	−31.4	345
80	348	−54.4	300
90	1000	−91.2	150

because there are only satellite-specific parameters in the adjustment—implying that the combined NEQ system de facto breaks up into s separate systems.

- An adjustment where all s direct SRP parameters *and* the geocenter offset G_3 are estimated would result in the correct D_0-values for every satellite and in the correct value for G_3. In the previously described experiment, these values would be $G_3 = 1$ m and $D_0 = 0$, thus also $\delta z = 0$, for all s satellites.
- The differences of the D_0-estimates from the two above adjustments (without and with estimating G_3) would therefore yield the offsets δz of Table C.1 (column 2), underlining the correctness of formula (28).

Table C.1 also supports the remarks in the main text: With longer arcs the variation in the angles β_s and thus the de-correlation of the two key parameters becomes substantial.

References

Altamimi, Z., Collilieux, X., Métivier, L. ITRF2008: an improved solution of the international terrestrial reference frame. J. Geod. 85 (8), 457–473, 2011.

Beutler, G., Brockmann, E., Gurtner, W., et al. Extended orbit modeling techniques at the CODE processing center of the International GPS Service for geodynamics (IGS): theory and initial results. Manuscr. Geod. 19, 367–384, 1994.

Beutler, G., Rothacher, M., Schaer, S., et al. The international GPS service (IGS): an interdisciplinary service in support of Earth sciences. Adv. Space Res. 23 (4), 631–653, 1999.

Beutler, G. Methods of Celestial Mechanics. Springer-Verlag, Berlin Heidelberg New York, 2005.

Bouillé, F., Cazenave, A., Lemoine, J.M., et al. Geocenter motion from the DORIS space system and laser data to the Lageos satellites: comparison with surface loading data. Geophys. J. Int. 143, 71–82, 2000.

Chen, J.L., Wilson, C.R., Eanes, R.J., et al. Geophysical interpretation of observed geocenter variations. J. Geophys. Res. 104 (B2), 2683–2690, 1999.

Dach, R., Hugentobler, U., Meindl, M., Fridez, P. (Eds.). The Bernese GPS Software Version 5.0. Astronomical Institute, University of Bern, Switzerland, 2007.

Dach, R., Brockmann, E., Schaer, S., et al. GNSS processing at CODE: status report. J. Geod. 83 (3–4), 353–366, 2009.

Dong, D., Dickey, J.O., Chao, Y., et al. Geocenter variations caused by atmosphere, ocean and surface ground water. Geophys. Res. Lett. 24 (15), 1867–1870, 1997.

Dow, J.M., Neilan, R.E., Rizos, C. The International GNSS Service in a changing landscape of global navigation satellite systems. J. Geod. 83 (3–4), 191–198, 2009.

Feissel-Vernier, M., LeBail, K., Berio, P., et al. Geocenter motion measured with DORIS and SLR, and predicted by geophysical models. J. Geod. 80, 637–648, 2006.

Ferland, R., Piraszewski, M. The IGS-combined station coordinates, earth rotation parameters, and apparent geocenter. J. Geod. 83 (3–4), 385–392, 2009.

Gobinddass, M.L., Willis, P., de Viron, O., et al. Systematic biases in DORIS-derived geocenter time-series related to solar radiation pressure mis-modeling. J. Geod. 83, 849–858, 2009.

Kang, Z., Tapley, B., Chen, J., et al. Geocenter variations derived from GPS tracking of the GRACE satellites. J. Geod. 83, 895–901, 2009.

Lavallée, D.A., van Dam, T., Blewitt, G., et al. Geocenter motions from GPS: a unified observation model. J. Geophys. Res. 111, B05405, 2006.

Meindl, M. Combined analysis of observations from different global navigation satellite systems. In: Geodätisch-geophysikalische Arbeiten in der Schweiz, vol. 83, Eidg. Technische Hochschule Zürich, Switzerland, 2011.

Mendes, V.B., Pavlis, E.C. High-accuracy zenith delay prediction at optical wavelengths. Geophys. Res. Lett. 31, L14602, 2004.

Moore, P., Wang, J. Geocentre variation from laser tracking of LAGEOS1/2 and loading data. Adv. Space Res. 31 (8), 1927–1933, 2003.

Ray, J. (Ed.). IERS analysis campaign to investigate motions of the geocenter. IERS Technical Note 25, Observatoire de Paris, 1999.

Springer, T.A., Beutler, G., Rothacher, M. A new solar radiation pressure model for GPS satellites. GPS Sol. 3 (2), 50–62, 1999.

Thaller, D., Sośnica, K., Dach, R., et al. Geocenter coordinates from GNSS and combined GNSS-SLR solutions using satellite co-locations. In: IAG Symp., vol. 139, in press.

Watkins, M., Eanes, R. Observations of tidally coherent diurnal and semidiurnal variations in the geocenter. Geophys. Res. Lett. 24 (17), 2231–2234, 1997.

Wu, X., Ray, J., van Dam, T. Geocenter motion and its geodetic and geophysical implications. J. Geodyn. 58, 44–61, 2012.